

PAPER

# Multidimensional nanofibrous hydrogels integrated triculture system for advanced myocardial regeneration

To cite this article: Dongwoo Kim *et al* 2025 *Biofabrication* **17** 015045

View the [article online](#) for updates and enhancements.

## You may also like

- [Mesenchymal stem cells for tissue engineering and regenerative medicine](#)  
Suk-Kee Tae, Seok-Hyn Lee, Jae-Sik Park et al.
- [Engineering highly-aligned three-dimensional \(3D\) cardiac constructs for enhanced myocardial infarction repair](#)  
Kang Han, Jiankang He, Liyan Fu et al.
- [bFGF binding cardiac extracellular matrix promotes the repair potential of bone marrow mesenchymal stem cells in a rabbit model for acute myocardial infarction](#)  
Guang-Wei Zhang, Tian-Xiang Gu, Xiao-Yu Guan et al.

# Biofabrication



## PAPER

# Multidimensional nanofibrous hydrogels integrated triculture system for advanced myocardial regeneration

Dongwoo Kim<sup>1,3</sup>, Yeong Hwan Kim<sup>2,3</sup>, Gyubok Lee<sup>1</sup>, Eun-Cheol Lee<sup>2</sup>, Suk Ho Bhang<sup>2,\*</sup> and Kangwon Lee<sup>1,\*</sup> 

<sup>1</sup> Department of Applied Bioengineering, Graduate School of Convergence Science and Technology, Seoul National University, Seoul 08826, Republic of Korea

<sup>2</sup> School of Chemical Engineering, Sungkyunkwan University, Suwon 16419, Republic of Korea

<sup>3</sup> Co-first authors: These authors contributed equally to this work.

\* Authors to whom any correspondence should be addressed.

E-mail: [sukhobhang@skku.edu](mailto:sukhobhang@skku.edu) and [kangwonlee@snu.ac.kr](mailto:kangwonlee@snu.ac.kr)

**Keywords:** multidimensional nanofibrous hydrogel, myocardial regeneration, triculture system

Supplementary material for this article is available [online](#)

RECEIVED  
4 September 2024

REVISED  
15 November 2024

ACCEPTED FOR PUBLICATION  
10 December 2024

PUBLISHED  
6 January 2025

## Abstract

Myocardial infarction (MI) remains a leading cause of mortality worldwide, posing a significant challenge to healthcare systems. The limited regenerative capacity of cardiac tissue following MI results in chronic cardiac dysfunction, highlighting the urgent need for innovative therapeutic strategies. In this study, we explored the application of a multidimensional nanofibrous hydrogel for myocardial regeneration. We developed a composite hydrogel system by integrating fibrin, polycaprolactone (PCL), and alginate. In this system, fibrin supported cell proliferation and significantly enhanced angiogenesis when combined with human umbilical vein endothelial cells (HUVECs). PCL contributed to the alignment of encapsulated cells, improving their organization within the scaffold. Adipose-derived stem cells (ADSCs) were encapsulated within the hydrogel for their versatile regenerative potential, while C2C12 cells were incorporated for their ability to form muscle tissue. Additionally, the inclusion of alginate not only enhanced the mechanical properties of the hydrogel to better match the biomechanical demands of cardiac tissue but also played a critical role in reducing the immune response, thereby improving the system's biocompatibility. This study presents an advanced platform for myocardial regeneration using a nanofibrous hydrogel system designed to meet the dual requirements of mechanical robustness and cellular compatibility essential for cardiac tissue engineering. The triculture system, consisting of ADSCs, C2C12 cells, and HUVECs, harnesses the regenerative capabilities of each cell type, promoting both angiogenesis and tissue regeneration. This comprehensive approach addresses the immediate needs for cellular survival and integration while effectively overcoming long-term mechanical and immunological challenges.

## 1. Introduction

Cardiovascular diseases, particularly myocardial infarction (MI), represent a leading cause of mortality worldwide, highlighting a significant burden on global health systems [1]. The heart's inherent inability to regenerate damaged myocardial tissue post-infarction leads to progressive cardiac dysfunction and failure [2]. This challenge underscores the urgent need for innovative therapeutic approaches that extend beyond current clinical management,

which primarily focuses on symptom relief and the prevention of further cardiac decline. Treatments such as percutaneous coronary intervention and coronary artery bypass grafting, alongside pharmacological interventions, primarily aim to preserve remaining cardiac function rather than restore lost myocardial tissue, as detailed by multiple sources [3, 4]. While these strategies aim to preserve remaining cardiac function and prevent additional damage, they do not address the restoration of lost myocardial tissue.

Advancements in MI therapy have increasingly relied on tissue engineering and regenerative medicine [5], exploring the potential of biomaterials [6, 7], stem cell therapy [8, 9], and scaffold-based cardiac repair [10–12]. These innovative methods aim to address the limitations of traditional treatments by promoting the regeneration of cardiac tissues through cellular therapies and bioactive scaffolds. However, challenges remain in achieving the integration and functional performance of engineered tissues within the host environment [13].

According to Chen *et al*, polyurethane/cellulose-based hydrogels demonstrate excellent cell retention and proliferation properties; however, their high young's modulus (1.5–87.2 MPa) presents limitations for myocardial applications [14]. In contrast, Roshanbinfar *et al* found that collagen hydrogels with polyethyleneimine-gold nanoparticles exhibit low mechanical stability (91.99–146.22 Pa), which can limit their suitability as myocardial patches [15]. The target young's modulus for myocardium regeneration is approximately 18–55 kPa, as suggested by Berry *et al* [16]. In this study, we developed a multi-dimensional nanofibrous hydrogel with a modulus of  $33 \pm 8.31$  kPa, closely matching the mechanical properties of native myocardium and making it well-suited for cardiac applications.

To address these challenges, we introduce a composite scaffold composed of fibrin, polycaprolactone (PCL), and alginate, each selected for its unique properties that support myocardial regeneration. PCL has been integrated into cardiac repair hydrogels for its high porosity and biocompatibility, which enhance cellular infiltration and integration within myocardial tissue. Fibrin, recognized for its role in wound healing, provides a natural scaffold that supports cell attachment and proliferation, creating an ideal environment for initiating tissue repair [17, 18]. According to Jarrell and Jacot, PCL-fibrin composites are beneficial for fostering angiogenesis and improving tissue integration in myocardial repair [19]. However, fibrin's pro-inflammatory potential presents a challenge when exposed directly *in vivo*. To counter this, we employed a PCL-Fibrin-Alginate tri-layer structure, incorporating alginate for its anti-inflammatory properties, which protect fibrin from direct exposure, thereby balancing vascular regeneration with immune modulation. Alginate plays a crucial role in further enhancing the scaffold's functionality by improving mechanical stability, minimizing the immune response, and modulating the scaffold's mechanical properties to match the surrounding tissue, promoting better integration and function [20, 21].

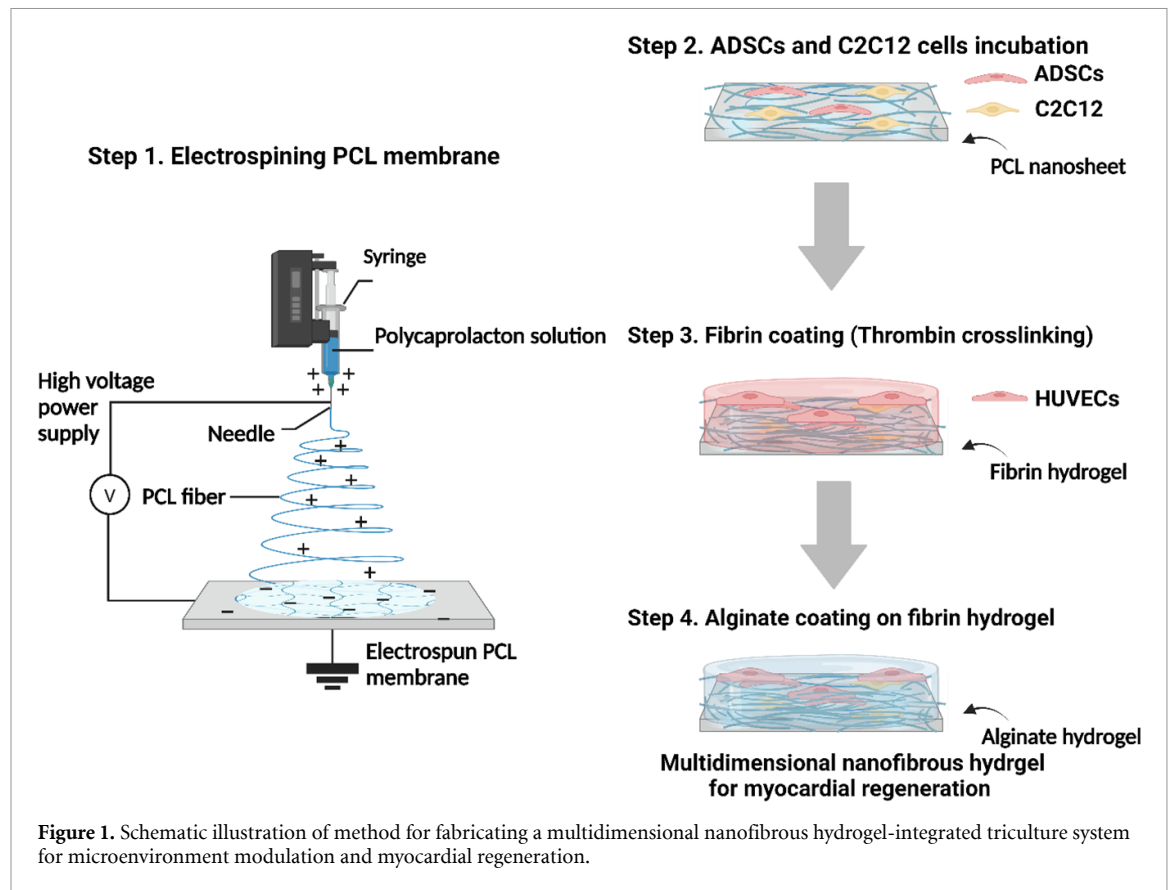
This study employs a triculture system composed of adipose-derived stem cells (ADSCs), C2C12 cells, and HUVECs, each selected for specific regenerative properties. ADSCs are used for

their immunomodulatory effects and angiogenic therapeutic potential [22]. Although C2C12 cells are not cardiac-derived, several studies have demonstrated their potential in cardiac regeneration, supporting their inclusion as an exploratory model in this proof-of-concept study. For instance, C2C12 cells combined with selenium nanoparticles, alginate, and pectin have been shown to form a biocompatible scaffold exhibiting antioxidative properties, enhanced mechanical strength, and cellular behaviors suited for cardiac tissue engineering applications [23]. Moreover, research shows that C2C12 cells transplanted into the myocardium of syngeneic mice successfully differentiate into myotubes and survive for up to three months, indicating their adaptability to cardiac environments [24]. C2C12 cells can also achieve alignment in microgrooved structures, mimicking myocardial organization and promoting structural integration [25], and have demonstrated cardiac-like sodium currents when exposed to a cardiac cell environment [26]. Additionally, C2C12 cells, when co-cultured with human umbilical vein endothelial cells (HUVECs), enhance endothelial network formation and angiogenesis and secrete pro-angiogenic factors through properties, they often require complex culture conditions and lengthy maturation times, making C2C12 cells a practical choice for initial proof-of-concept studies [27].

The success of these engineered tissues depends heavily on vascularization, which is why HUVECs have been incorporated [28, 29]. HUVECs facilitate the formation of new blood vessels, ensuring the scaffold supplies adequate nutrients and oxygen, critical for the survival and integration of regenerated tissues. The synergy between fibrin and HUVECs enhances angiogenesis within the scaffold, thereby boosting the scaffold's effectiveness in supporting regenerative processes.

The layered structure of our scaffold is designed to address the complex demands of myocardial regeneration, with each layer performing specific functions that collectively contribute to the recovery of heart tissue. In this study, we fabricate a myocardial regeneration platform using multidimensional nanofibrous hydrogels, designed to meet the dual requirements of mechanical robustness and cellular compatibility essential for cardiac tissue engineering (figure 1). Our approach integrates biocompatible materials with cellular engineering to develop a scaffold that balances mechanical compliance with the strength necessary to withstand cardiac stresses.

We conducted thorough evaluations of the hydrogel's mechanical properties, swelling ratio, and biocompatibility, ensuring that it supports both the physical and biological aspects of myocardial repair. The triculture system, composed of ADSCs, C2C12 cells, and HUVECs, exploits the regenerative potential of each cell type to promote angiogenesis and



muscle tissue formation, thereby enhancing the scaffold's overall functionality. A key feature of the scaffold is the inclusion of alginate to modulate the immune response, a crucial factor in minimizing inflammation and ensuring long-term implantation success. This was validated *in vivo* using a rat MI model, where the scaffold demonstrated significant capability in tissue integration and regeneration.

Our research advances the field of cardiac regeneration by presenting a scaffold that not only meets the immediate requirements for cell survival and integration but also addresses long-term challenges related to mechanical and immunological compatibility. This approach underscores the scaffold's potential to transform regenerative therapies in cardiology, setting a new benchmark for future efforts in cardiac tissue engineering.

## 2. Materials and methods

### 2.1. Cell culture

Human ADSCs were purchased from CEFO (Seoul, Republic of Korea). HUVECs were purchased from Lonza Inc. (Bazel, Switzerland), while C2C12 cells were sourced from the Korean Cell Line Bank (Seoul, Republic of Korea). The cells were maintained in T-75 flasks at 37 °C under a humidified atmosphere containing 5% CO<sub>2</sub> until they were utilized for experiments. ADSCs and C2C12 cells were cultured using Dulbecco's Modified Eagle's Medium (DMEM),

supplemented with 1% penicillin-streptomycin (Welgene, Gyeongsan, Republic of Korea) and 10% FBS (Cellsera, Australia). HUVECs were cultured using Endothelial Basal Medium (EBM-2, Lonza) supplemented with Endothelial Growth Supplement Single Quots (EGM-2, Lonza) and 1% v/v antibiotic-antimycotics.

### 2.2. Preparation of multidimensional nanofibrous hydrogel

To fabricate the hydrogels for myocardial regeneration, PCL fibers were initially generated through the electrospinning method. Initially, a 20 wt% PCL solution (Molecular Weight: 80 000 g mol<sup>-1</sup>, Sigma Aldrich, St. Louis, MO, USA) dissolved in 2,2,2-trifluoroethanol was extruded via a syringe pump from a 7.5 kV positive voltage-applied 18G metal needle at a consistent rate (0.8 ml h<sup>-1</sup>) for a duration of 30 min. The electrospun PCL membrane was cut into 5 mm square shapes and placed on the bottom of a 96-well plate. Subsequently, 1.25 × 10<sup>5</sup> of ADSCs and C2C12 cells were each dispersed in 20 μl of DMEM, and dispensed onto the PCL membrane, followed by incubation for 30 min at 37 °C in a 5% CO<sub>2</sub> environment. Immediately afterwards, 2.5 × 10<sup>5</sup> cell of HUVECs were dispersed in 80 μl of fibrin precursor solution (20 mg ml<sup>-1</sup> in 3 w/v % NaCl) and dispensed onto the membrane. Then, 8 μl of thrombin (2.5 U ml<sup>-1</sup> in 20 mM CaCl<sub>2</sub>) was added to facilitate crosslinking. After extracting the PCL-fibrin

hybrid scaffold using a micro spoon spatula, a secondary layer of alginate hydrogel was applied to encase the fibrin hydrogel. In brief, the retrieved PCL-fibrin hybrid scaffold was submerged in 6-well plate containing 5 ml of 1 wt% sodium alginate hydrogel precursor solution, and 5 ml of a 1 wt% calcium chloride solution was introduced for 30 s at room temperature to facilitate alginate crosslinking.

### 2.3. Characterization of multidimensional nanofibrous hydrogel

The mechanical characteristics of the multidimensional nanofibrous hydrogels were evaluated by carrying out assessments on the compressive modulus of the fibrin hydrogel, PCL-fibrin hybrid scaffold, and the multidimensional nanofibrous hydrogels scaffolds themselves using Instron 3343 universal testing system (Instron Corp., Norwood, MA, USA). Each scaffold was submerged in phosphate buffered saline (PBS, Welgene) to undergo swelling for a period of 30 min. Subsequently, any surplus fluid was removed diligently to prepare the scaffolds for analysis. They were then placed on the testing machine and subjected to a compressive force. Both the compressive stress and strain exerted on the scaffolds were recorded. From these measurements, calculations were made to determine the true stress and strain values. The viscoelastic property of the scaffolds was analyzed thoroughly using a dynamic shear modulus deformation approach. The specimens were positioned carefully between a metal plate measuring 2 cm, maintaining a gap of 1 cm between them [30]. Their vibration-shear deformation was evaluated using a rheometer (MCR 102, Anton Paar, Graz, Australia). The storage modulus of the samples was determined by subjecting them to a continuous deformation mode, applying a consistent strain of 10% across a frequency range of 0.1–300 Hz ( $\text{rad s}^{-1}$ ), all at a controlled temperature of 25 °C.

### 2.4. Swelling test

To assess the water uptake and retention capabilities as an implantable hydrogel for myocardial regeneration, the swelling capacity was measured at 37 °C. The hydrogel samples were dried in a 70 °C oven overnight and then rehydrated in PBS. Excess PBS present on the surface of the hydrogel was absorbed using filter paper, and the samples were weighed three times to obtain reliable data. The swelling ratio of the hydrogels was calculated using the formula  $(W_t - W_0)/W_0 \times 100$ , where  $W_t$  represents the weight of the swollen hydrogel at a specific time, and  $W_0$  denotes its initial dry weight, providing a quantitative measure of the hydrogel's fluid absorption and retention capacity.

### 2.5. Scanning electron microscope (SEM) imaging

The external structures of the scaffold were examined using SEM from Helios 5 UC (FEI, ThermoFisher,

Waltham, MA, USA). A layer of platinum was coated on the scaffolds through a sputter-coating process prior to this analysis. The SEM investigation was conducted under an acceleration voltage of 10 kV to ensure high-resolution imagery and detailed insight into the scaffold's surface topography.

### 2.6. Compatibility test

The compatibility of the hydrogel composite against ADSCs, HUVECs, and C2C12 cells was evaluated by using hydrogel extracts. Briefly, hydrogel extracts were prepared by swelling the hydrogel composite in serum free media at a concentration of  $0.2 \text{ g ml}^{-1}$  in an incubator for 48 h at 37 °C. For live and dead assay, ADSCs, HUVECs, and C2C12 cells were seeded at a density of  $5 \times 10^4$  cells per well on 24-well plates for 48 h. After treating the cells with hydrogel extract solution in the same manner as described above, the cell viability at day 1, 4, and 7 were observed by adding  $2 \mu\text{M}$  calcein acetoxymethylester (AM) and  $4 \mu\text{M}$  ethidium homodimer-1. To assess cell cytotoxicity within the scaffolds in a direct manner when cells were present inside the scaffold, ADSCs, HUVECs, and C2C12 cells were individually inserted and cultured within the scaffolds for 7 d. Subsequently, the cells were treated with calcein AM and  $4 \mu\text{M}$  ethidium homodimer-1 for 30 min, and fluorescence images were obtained (Carl Zeiss, Oberkochen, Germany).

### 2.7. *In vitro* cell proliferation test

The *in vitro* cell proliferation study over the scaffold for myocardial regeneration were carried out by EZ-Cytox (DoGenBio, Seoul, Republic of Korea). In brief, scaffold extracts were prepared by swelling the scaffold composite in the media containing 10% FBS serum at a concentration of  $0.2 \text{ g ml}^{-1}$  in an incubator for 48 h at 37 °C. Scaffolds were sterilized in 0.1% (v/v) peracetic acid (Sigma-Aldrich, USA) and the scaffolds were rinsed in sterile PBS for 3 h. ADSCs, HUVECs and C2C12 cells were seeded at a density of  $5 \times 10^4$  cells per well on 24-well plates for 48 h. After treating the cells with hydrogel extract solution in the same manner as described above, the cell proliferation at day 1, 4, and 7 were observed by adding water soluble tetrazilium salt solution at 30 min, and the absorbance was measured at 450 nm using a microplate reader (Synergy H1, BioTek, VT).

### 2.8. Quantitative reverse transcription polymerase chain reaction (qRT-PCR)

qRT-PCR was used to quantify the relative expression levels of genes. The samples were lysed in TRIzol™ reagent (Invitrogen, Carlsbad, CA, USA), and total RNA was extracted with chloroform and precipitated with isopropanol. After the supernatant was removed, the RNA pellet was washed with 75% (v/v) ethanol, air-dried, and dissolved in 0.1% (v/v) diethyl pyrocarbonate-treated water. For qRT-PCR, the SsoAdvanced™ Universal SYBR Green Supermix

Kit (Bio-Rad, Hercules, CA, USA) and the CFX Connect™ real-time PCR Detection System (Bio-Rad) were used. The primer sequence is described in supplementary data.

### 2.9. Tube formation test

The angiogenic potential of the scaffold for myocardial regeneration was evaluated in a controlled setting using an *in vitro* tube formation assay. Initially, growth factor-reduced Matrigel (Corning Incorporated, New York, NY, USA) was evenly spread across each well to form a basement membrane matrix layer. The coated well plate underwent incubation at room temperature for 30 min, followed by further incubation in a humidified atmosphere (5% CO<sub>2</sub>, 37 °C) for 1 h. HUVECs were then seeded onto the 2D bottom surface of each well. These HUVECs were cultured for 16 h in a transwell system, with cell-encapsulated hydrogels placed in the upper chamber, containing HUVECs alone, HUVECs with ADSCs, and HUVECs with ADSCs and C2C12 cells. After 16 h of incubation, the tubular structures formed on the 2D surface were imaged using a microscope. ImageJ software was used to count the tubular nodes and junctions observed in these images.

### 2.10. Enzyme-linked immunosorbent assay (ELISA)

In 24-well plates, mouse macrophages were cultured at a density of  $5 \times 10^4$  cells per well for a period of 24 h to prepare for proinflammatory cytokine analysis via ELISA. Post-incubation, the cells were exposed to a variety of scaffold eluates. Following a 24 h period of treatment, the supernatant was collected from these cultures and centrifuged to remove any cellular debris. After centrifugation, the concentrations of TNF- $\alpha$  (Abcam, Cambridge, UK), IL-1 $\beta$  (Abcam), and IL-6 (Abcam) cytokines were quantitatively determined using specific ELISA kits.

### 2.11. Western blot assay

The RAW 264.7 macrophage cell line (ATCC, Manassas, VA, USA) was cultured and subjected to treatment with various scaffold elutes for durations of 6 and 24 h. After the treatment, the cells were washed and lysed with RIPA buffer, which was augmented with Xpert phosphatase inhibitor cocktail solution (GenDEPOT, Barker, TX, USA). Proteins from the cells were then resolved by 10% SDS-PAGE and transferred onto PVDF membranes. These membranes were blocked using 5% skim milk and then incubated with primary antibodies. The antibodies used included  $\beta$ -Actin (Cell Signaling Technology, Danvers, MA, USA), TGF- $\beta$  (Cell signaling), IL-1 $\beta$  (Abcam), and CD206 (Abcam). After the incubation with primary antibodies, the membranes were incubated with a secondary antibody (Abcam). The protein bands were visualized on the PVDF membranes using a Las 4000 device (Fujifilm Life Science,

Tokyo, Japan) in conjunction with Clarity Western ECL substrate (Bio-Rad).

### 2.12. MI model

8-week-old female SD-rats (180–200 g, DBL) were anaesthetized by inhalation of 2% isoflurane (Ifiran®, Hana Pharm. Co. Seoul, Republic of Korea). The rats were intubated with an intravenous catheter (18G) for mechanical ventilation. After a left thoracotomy, the ligation of the left anterior descending artery was performed with suture (7–0 Prolene, Ethicon, San LORENZO, Puerto Rico) to induce MI. Patches were attached around infarction site with fibrin adhesive (Greenplast®, GreenCross Co., Yongin, Republic of Korea). The handling of all animals was approved and certified by the Institutional Animal Care and Use Committee at Sungkyunkwan University (SKKUIACUC2021-12-14-2).

### 2.13. Histological examination

The cardiac tissues that were retrieved at 3 d for immune analysis and 28 d for cardiac regeneration post-surgery were embedded in optimal cutting temperature compound (SciGen Scientific Inc., Gardenas, CA, USA). The samples were frozen at  $-20$  °C and sliced into 10  $\mu$ m-thick sections using a microtome (Cryostat, Leica). The sliced samples were stained with hematoxylin and eosin (H&E) to verify tissue regeneration and with Masson's Trichrome (MT) staining to assess fibrosis.

### 2.14. Terminal deoxynucleotidyl transferase dUTP nick end labeling (TUENL) assay

To observe the apoptotic activity of cardiac tissue, the Fluorescein *In Situ* Apoptosis Detection Kit (Merck Millipore, Darmstadt, Germany) was used according to the manufacturer's instructions. The final fluorescence images were captured using a fluorescence microscope (DMi8).

### 2.15. Immunohistochemistry

The sliced samples were stained with primary antibodies targeting anti-cTnT, anti-CD31, anti-CD68, anti-NOS2, and anti-CD206 antibodies (all antibodies were purchased from Cell Signaling Technology). After staining with the primary antibodies, fluorescein isothiocyanate-conjugated anti-rabbit antibodies (Cell Signaling Technology) were used to detect the signals. The immunohistochemically stained samples were counterstained with DAPI, and the images were obtained using a fluorescence microscope (DMi8). Image analysis and fluorescence intensity quantifications were performed using ImageJ (National Institutes of Health, USA).

### 2.16. Hypoxic and normoxic cell culture condition for ADSCs, HUVECs, C2C12 cells tri-culture

ADSCs and C2C12 cells were seeded at a density of  $1.25 \times 10^5$  cells each, and HUVECs at a density of

$2.5 \times 10^5$  cells, in a 6-well plate and cultured for 2 d. Following this initial culture period, the cells were incubated for 30 min at 37 °C in a 5% CO<sub>2</sub> atmosphere. Normoxic conditions were maintained with 18% O<sub>2</sub>, while hypoxic conditions were set at 2% O<sub>2</sub>, in cell culture dishes as described in prior study [31].

### 2.17. Statistical analysis

Data are presented as mean  $\pm$  standard deviation. The analysis was conducted with the aid of GraphPad Prism 8 software (GraphPad, San Diego, CA). Statistical significance was evaluated using one-way ANOVA with Tukey's test, and the significance of differences was set at \*  $p < 0.05$ .

## 3. Result

### 3.1. Characterization of multidimensional nanofibrous hydrogel for myocardial regeneration

The multidimensional nanofibrous hydrogel developed for myocardial regeneration was extensively characterized for its structural, mechanical, and swelling properties. The hydrogel's structure was analyzed using SEM and digital camera imaging, revealing well-organized compartmentalization of PCL fibers, fibrin gel, and alginate. SEM images (figure 2(a)) provided a detailed view of the scaffold's microarchitecture, illustrating the fine alignment of PCL fibers within the fibrin matrix and the seamless encapsulation by the outer alginate layer. Digital camera images (figure 2(b)) further demonstrated the uniform distribution and integration of these components within the hydrogel. Additionally, the diameter of the fibrin layer alone is  $2.72 \pm 0.25$  mm, while the hydrogel including the alginate layer measures  $3.86 \pm 0.19$  mm, with the alginate coating layer itself being 1.14 mm thick (figure S1).

The compressive modulus of the hydrogel was measured to assess its mechanical strength. As shown in figure 2(c), the fibrin hydrogel exhibited a compressive modulus of  $3.60 \pm 0.37$  kPa, which, while suitable for supporting cell proliferation, was insufficient to withstand the dynamic mechanical forces experienced in the heart [32]. The integration of PCL fibers significantly enhanced the compressive modulus to  $5.92 \pm 1.78$  kPa, providing improved structural integrity. With the addition of an alginate coating, the compressive modulus increased further to  $33 \pm 8.31$  kPa. These findings are supported by dynamic rheology measurements (figure 2(d)), which showed that the storage modulus of the PCL-embedded fibrin hydrogel with alginate coating remained consistently higher across all tested frequencies. Swelling tests were also conducted to evaluate the hydrogel's capacity to absorb and retain fluids, a critical property for sustaining cellular activities and facilitating nutrient transport within the scaffold. The swelling ratios of different hydrogel compositions were measured over time. As shown in

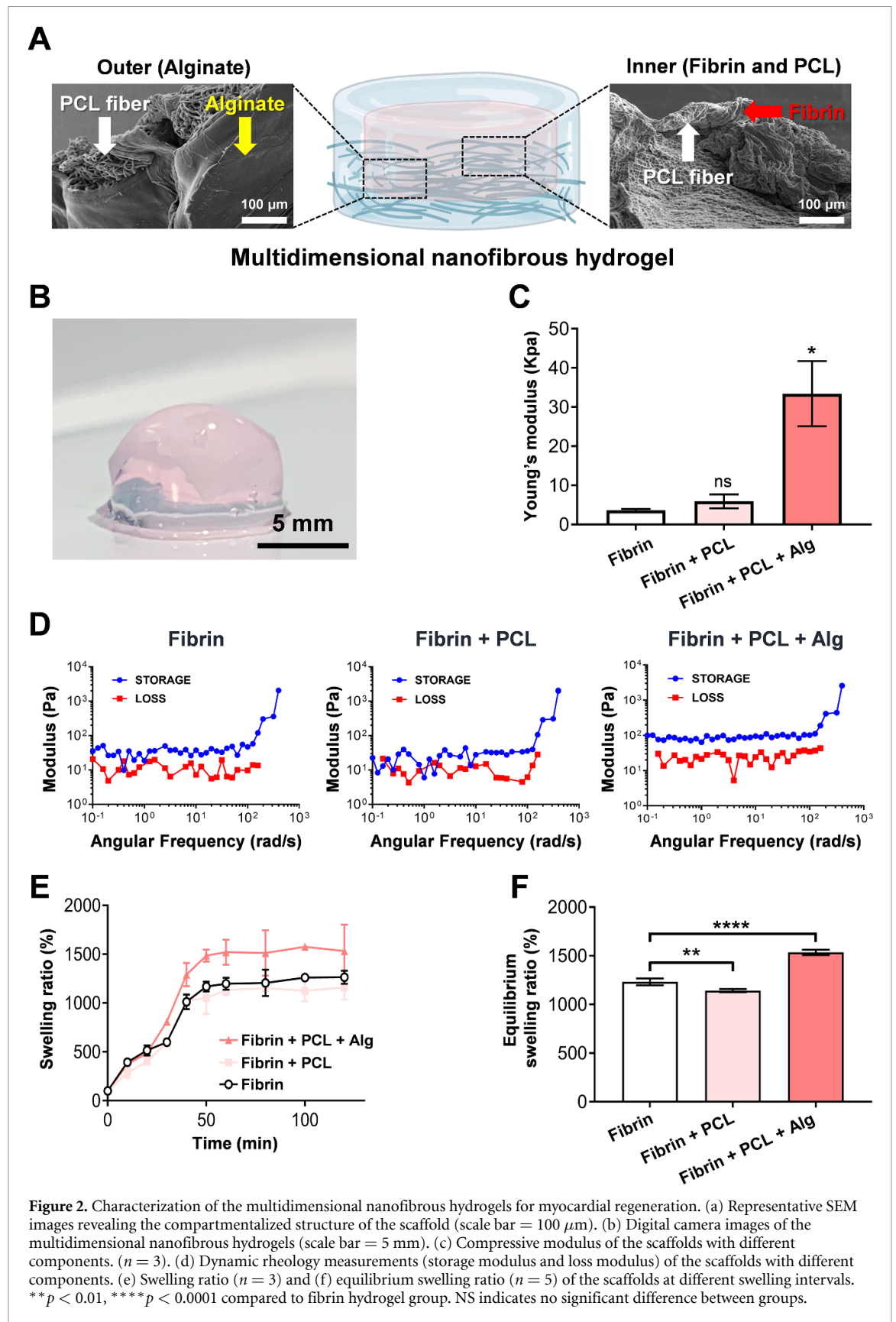
figure 2(e), the fibrin hydrogel alone reached an equilibrium swelling ratio of  $1231 \pm 35.18\%$ , demonstrating superior fluid retention but also suggesting the potential for excessive swelling, which could lead to structural instability. The incorporation of PCL fibers slightly reduced the swelling ratio to  $1142 \pm 16.30\%$ , indicating that the fibers provided some structural restraint against over-swelling. The alginate-coated hydrogel exhibited the highest equilibrium swelling ratio at  $1535 \pm 27.59\%$ , reflecting its enhanced capacity to retain moisture and nutrients, which is essential for cell survival and proliferation. This combination of high swelling capacity and mechanical robustness makes the alginate-coated hydrogel particularly well-suited for myocardial regeneration.

### 3.2. Assessment of compatibility of multidimensional nanofibrous hydrogel

The survival and proliferation of cells are critical indicators of the hydrogel's compatibility and its potential to support myocardial regeneration. To evaluate the cytocompatibility of the hydrogels, ADSCs, HUVECs, and C2C12 cells were cultured under both scaffold eluate and direct encapsulation conditions. As illustrated in figures 3(a)–(c), a high percentage of live cells (green) were observed across all cell types (ADSCs, HUVECs, and C2C12 cells) in the scaffold eluate. The absence of a significant red signal (dead cells) suggests that the hydrogel does not release cytotoxic substances and is highly biocompatible. Furthermore, cells directly encapsulated within the hydrogel were measured on days 1, 4, and 7 and showed no significant cytotoxic response. (figure 3(d)). These results demonstrate the hydrogel's ability to maintain a supportive microenvironment for cellular activities. The proliferation of ADSCs, HUVECs, and C2C12 cells within the hydrogel was monitored over a 7 d period using the EZ-Cytox assay. As shown in figure 3(e), all cell types exhibited smooth and continuous proliferation, with significant increases in cell numbers observed on days 4 and 7 compared to day 1. The triculture system (ADSCs, HUVECs, and C2C12 cells) displayed particularly robust proliferation, indicating that the hydrogel not only supports cell survival but also promotes active cell growth and division. This is critical for the regeneration of complex myocardial tissues, where the interaction between multiple cell types is necessary for the formation of functional tissue.

### 3.3. Assessment of regenerative potential of encapsulated cells in multidimensional nanofibrous hydrogel

In tissue engineering, 3D culture systems are increasingly recognized for their superior ability to replicate the human body's environment, providing enhanced cell-cell and cell-matrix interactions that are crucial for maintaining cellular functions and promoting tissue regeneration [33]. These enhanced interactions



in 3D systems lead to the upregulation of angiogenic factors, which are essential for effective tissue repair and angiogenesis [34]. In this study, we specifically evaluated the regenerative potential of a 3D triculture system, comprising ADSCs, HUVECs, and C2C12

cells, encapsulated within the multidimensional nanofibrous hydrogel, focusing on the mechanisms driving angiogenesis and the expression of critical regenerative factors (figure 4(a)). The hypoxic conditions simulated by the three-dimensional alginate-coated

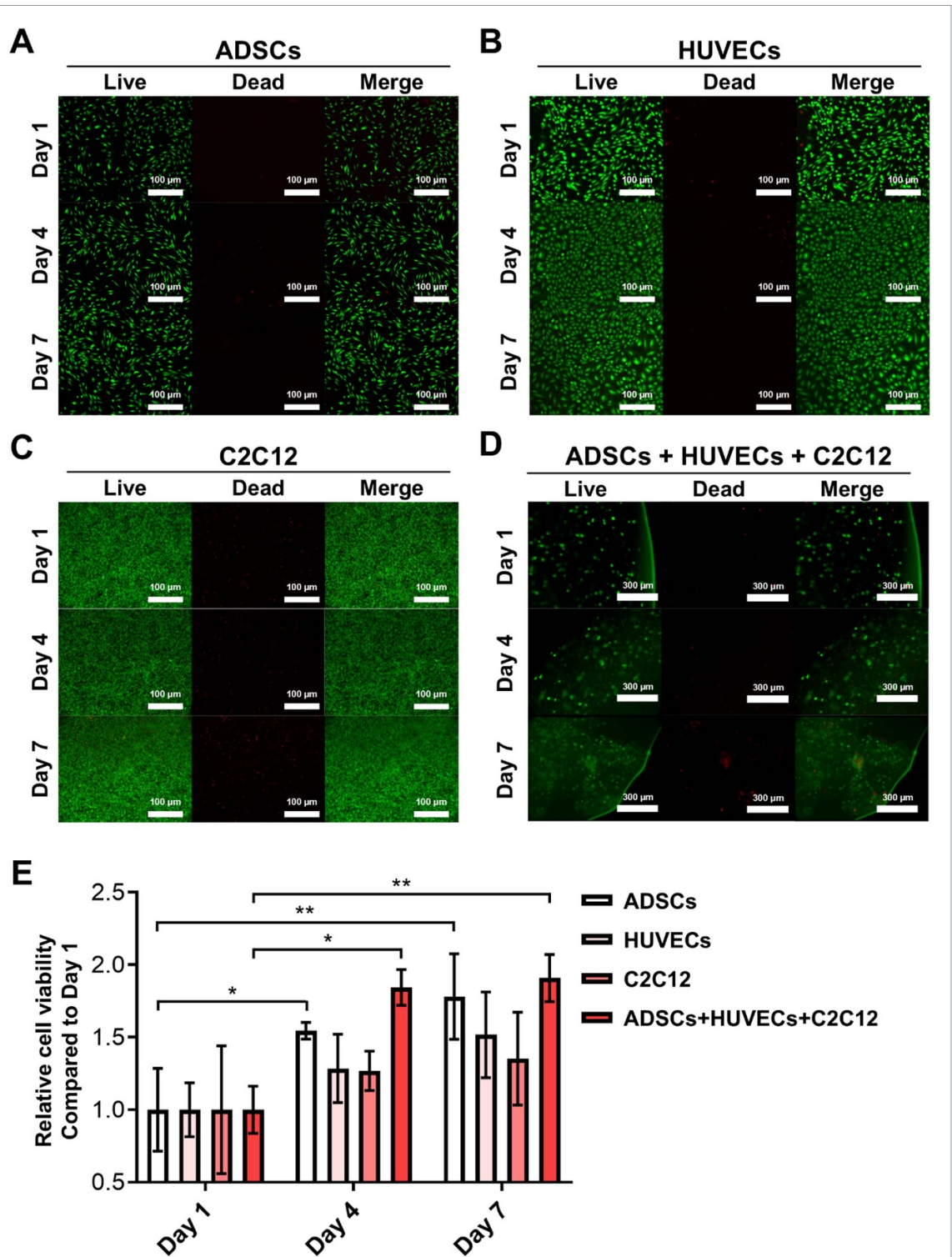
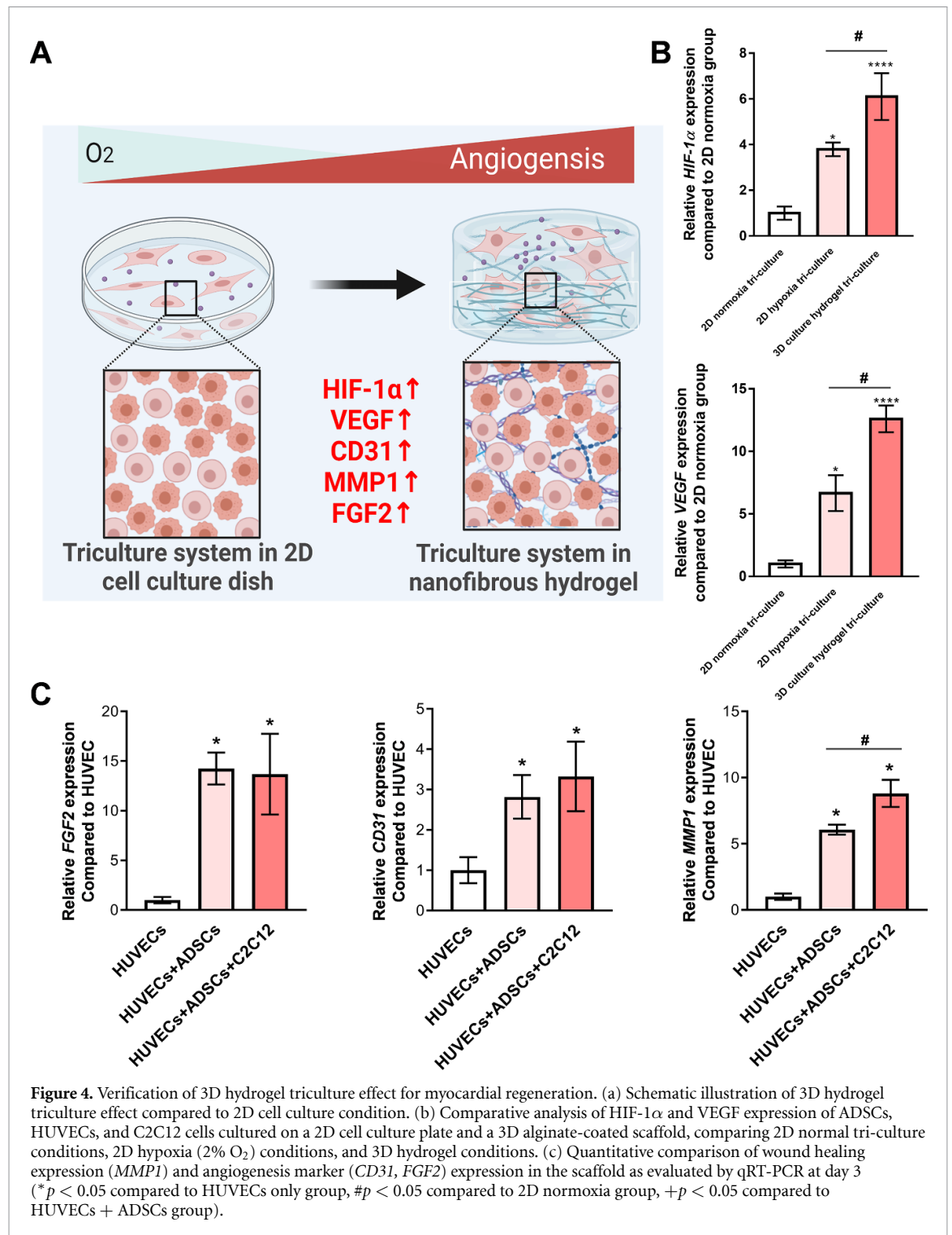


**Figure 3.** Compatibility evaluation of the multidimensional nanofibrous hydrogel for myocardial regeneration, with all fluorescence images captured on days 1, 4, and 7. (a) Fluorescence images of live (green) and dead (red) ADSCs in hydrogel eluate (Scale bar: 100  $\mu\text{m}$ ). (b) Fluorescence images of live and dead HUVECs in hydrogel eluate. (c) Fluorescence images of live and dead C2C12 in hydrogel eluate (scale bar: 100  $\mu\text{m}$ ). (d) Fluorescence images of live and dead ADSCs, HUVECs, and C2C12 cells directly encapsulated within the hydrogel (Scale bar: 300  $\mu\text{m}$ ). (e) Cell proliferation test of different cell types cultured in hydrogel eluates, using WST-based EZ-Cyto assay for indirect evaluation ( $n = 3$ , \* $p < 0.05$ , \*\* $p < 0.01$  compared to each group at day 1).

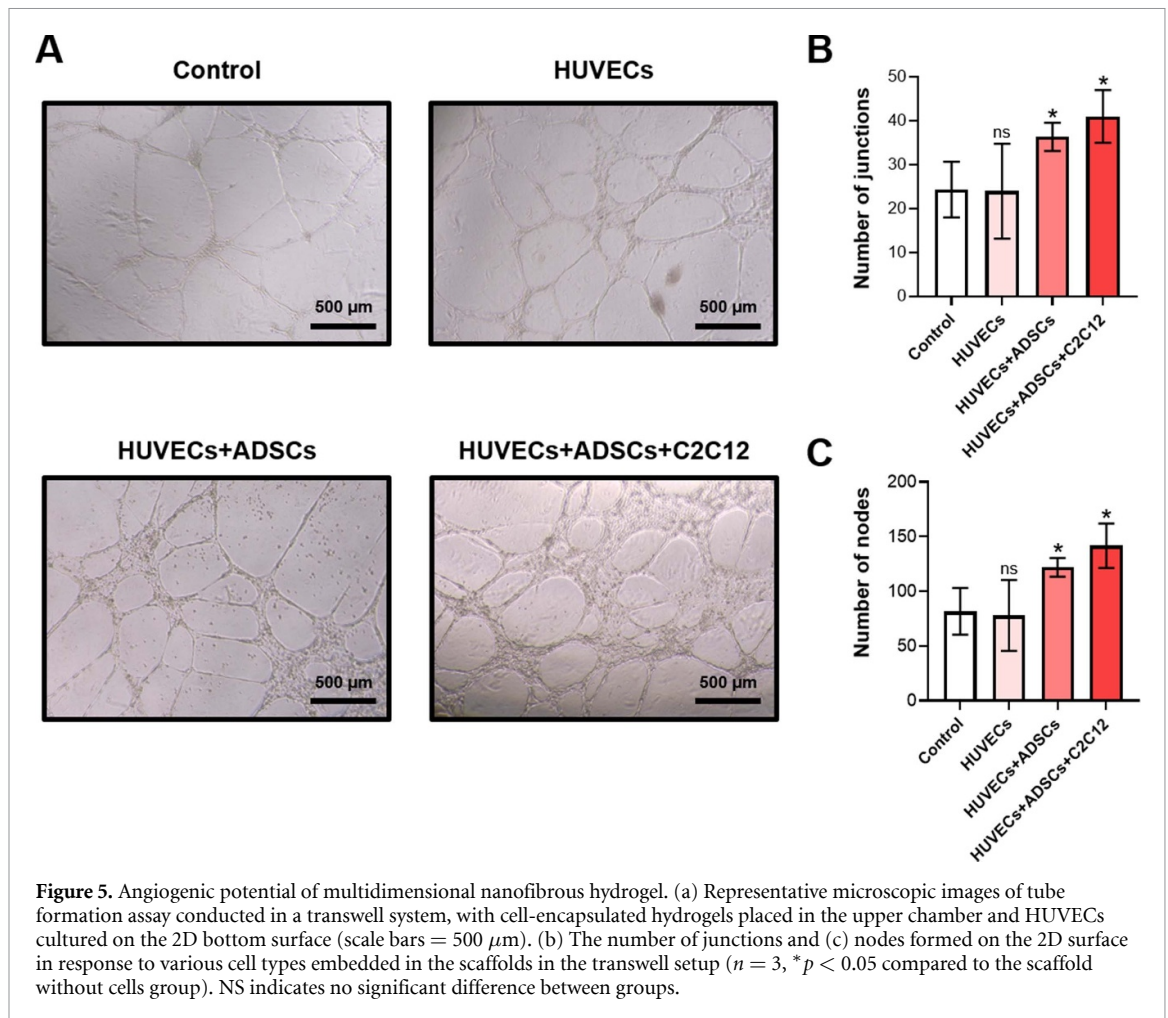
scaffold were shown to activate the HIF-1 $\alpha$ /VEGF pathway, which plays a critical role in promoting angiogenesis [35]. As shown in figure 4(b), The angiogenic potential under varying oxygen conditions was evaluated by comparing HIF-1 $\alpha$  and VEGF expression across 2D normoxia, 2D hypoxia, and 3D

hydrogel environments. HIF-1 $\alpha$  expression under 2D hypoxia increased 3.79-fold compared to 2D normoxia. This expression level was further enhanced in the 3D hydrogel, reaching a 6.09-fold increase over the 2D normoxic condition. VEGF expression followed a similar pattern, with a 6.656-fold increase



under 2D hypoxia and a 12.589-fold increase in the 3D hydrogel compared to 2D normoxia. These results suggest that, while hypoxic conditions alone enhance VEGF expression, the 3D hydrogel environment further amplifies this effect. This increase is likely due to the cell-cell interactions and cell-hydrogel interactions within the 3D scaffold, which create a more physiologically relevant microenvironment that mimics hypoxia and promotes angiogenic factor expression. This elevated gene expression under hypoxic conditions suggests that the scaffold

effectively mimics the *in vivo* myocardial environment, promoting the formation of new blood vessels, which are essential for tissue regeneration and survival. qRT-PCR was used to measure the expression levels of wound healing and angiogenic markers, including MMP1, CD31, and FGF2. As depicted in figure 4(c), co-encapsulation of ADSCs and HUVECs within the hydrogel significantly upregulated MMP1 expression to  $6.06 \pm 0.37$ -fold and CD31 expression to  $2.81 \pm 0.53$ -fold compared to the HUVEC-only group. The inclusion of C2C12 cells further amplified



these effects, with MMP1 expression increasing to  $8.80 \pm 1.02$ -fold and CD31 expression to  $3.32 \pm 0.86$ -fold. FGF2 expression also showed a notable increase, particularly in the ADSCs + HUVECs group, where it reached  $14.24 \pm 1.60$ -fold, slightly decreasing to  $13.68 \pm 4.05$ -fold with the addition of C2C12 cells. These findings underscore the synergistic effects of the triculture system in promoting the regenerative processes necessary for myocardial repair.

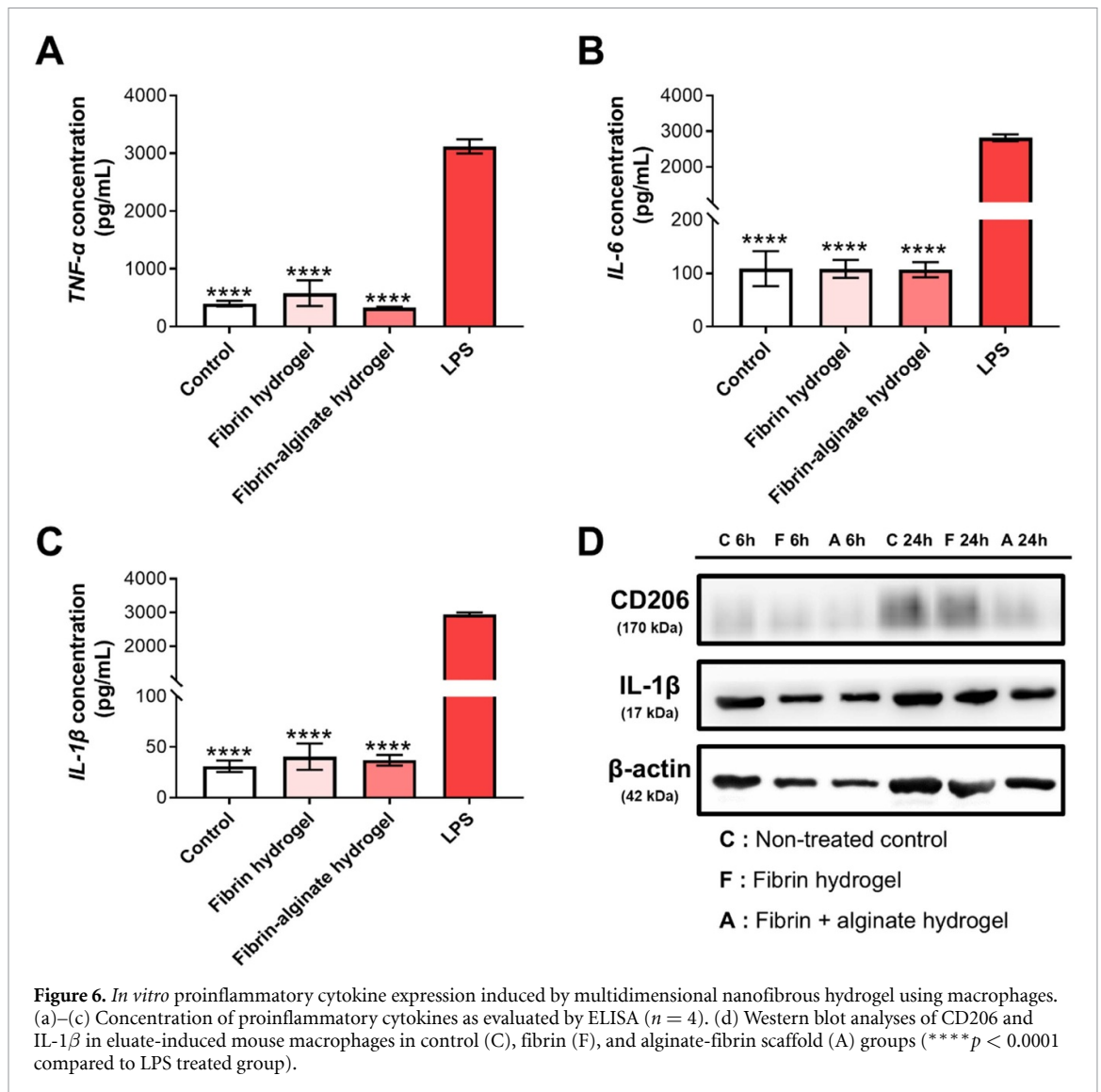
### 3.4. Evaluating angiogenic potential of multidimensional nanofibrous hydrogel

The angiogenic potential of the hydrogel system was further evaluated using a tube formation assay to assess the ability of HUVECs to form capillary-like structures in a transwell setup. In this configuration, the cell-encapsulated hydrogel was placed in the upper chamber, while HUVECs were cultured on the 2D bottom surface. As shown in figure 5(a), when HUVECs were cultured alone in the 2D setup with the control hydrogel (without cells) in the transwell, the number of junctions and nodes ( $24.0 \pm 10.81$ ) was not significantly different from the control hydrogel without cells ( $24.33 \pm 6.35$ ). These findings suggest that the presence of HUVECs alone is insufficient to enhance angiogenesis. However, when HUVECs

were co-cultured with ADSCs in the transwell system, there was a significant increase in both junctions ( $36.33 \pm 3.21$ ) and nodes, indicating a marked improvement in angiogenic potential. The addition of C2C12 cells to the hydrogel system further increased junction and node formation to  $41.0 \pm 6.0$ , as shown in figures 5(b) and (c). These results emphasize the critical role of the multicellular environment provided by the hydrogel in promoting the formation of a robust vascular network, which is essential for effective myocardial regeneration.

### 3.5. Evaluating inflammatory response induced by multidimensional nanofibrous hydrogel

The expression levels of representative proinflammatory cytokines, including TNF- $\alpha$ , IL-6, and IL-1 $\beta$ , were measured in macrophages exposed to the hydrogel components. As shown in figures 6(a)–(c), macrophages treated with fibrin and alginate-coated fibrin hydrogels exhibited proinflammatory cytokine levels comparable to the control group. Specifically, TNF- $\alpha$  levels in the fibrin hydrogel group were  $578.97 \pm 221.35$  pg ml $^{-1}$ , higher than the control group ( $399.56 \pm 49.48$  pg ml $^{-1}$ ), but lower than those in the LPS-treated group. The fibrin–alginate hydrogel group showed even lower



TNF- $\alpha$  levels at  $328.58 \pm 17.45 \text{ pg ml}^{-1}$ , suggesting that the alginate coating mitigates the inflammatory response induced by fibrin alone. For IL-6, the levels in the fibrin ( $108.00 \pm 16.68 \text{ pg ml}^{-1}$ ), control ( $108.67 \pm 32.84 \text{ pg ml}^{-1}$ ), and fibrin–alginate hydrogel ( $106.67 \pm 14.11 \text{ pg ml}^{-1}$ ) groups did not indicate a significant inflammatory response in any of the hydrogel-treated groups. These findings suggest that, despite a slight increase in TNF- $\alpha$  in the fibrin hydrogel group, the overall expression of proinflammatory cytokines is minimal, indicating that the hydrogel systems are generally biocompatible and unlikely to induce harmful inflammation. Western blot analysis further corroborated these results, showing that the expression of proinflammatory markers such as CD206 and IL-1 $\beta$  did not significantly increase in macrophages exposed to the hydrogel eluates (figure 6(d)). These results confirm that the hydrogel systems, particularly the alginate-coated fibrin hydrogel, maintain a low proinflammatory profile, making them suitable for potential tissue engineering applications.

### 3.6. Evaluating the myocardial regeneration induced by multidimensional nanofibrous hydrogel

Body weight and heart weight are important indicators of cardiac condition following MI, as significant weight loss and cardiac atrophy are commonly associated with severe heart damage. As shown in figure 7(a), the average body weight of MI-induced rats in the cell carrier group was  $280.67 \pm 9.04 \text{ g}$ , which was significantly higher than the  $254.83 \pm 11.89 \text{ g}$  observed in the non-treated (NT) group,  $258.08 \pm 10.05 \text{ g}$  in the carrier-only group, and  $251.33 \pm 16.88 \text{ g}$  in the cell-only group. This increase in body weight suggests that the animals in the cell carrier group experienced less systemic deterioration and better overall health, likely due to improved cardiac function. Heart weight analysis revealed similar results. The average heart weight in the cell carrier group was  $1.52 \pm 0.14 \text{ g}$ , compared to  $1.22 \pm 0.06 \text{ g}$  in the NT group,  $1.23 \pm 0.05 \text{ g}$  in the carrier-only group, and  $1.21 \pm 0.08 \text{ g}$  in the cell-only group. The higher heart weight in the cell carrier

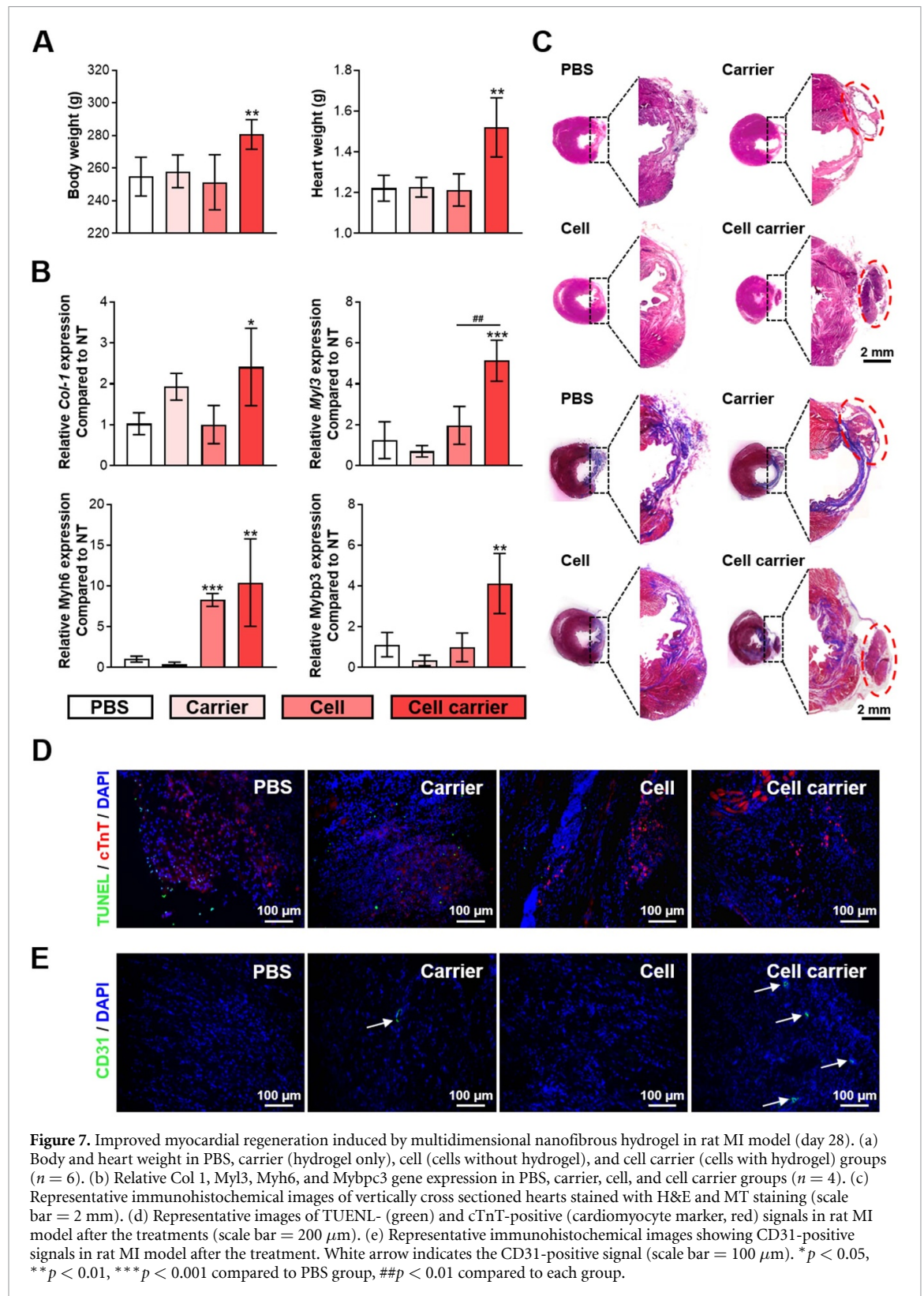


**Figure 7.** Improved myocardial regeneration induced by multidimensional nanofibrous hydrogel in rat MI model (day 28). (a) Body and heart weight in PBS, carrier (hydrogel only), cell (cells without hydrogel), and cell carrier (cells with hydrogel) groups ( $n = 6$ ). (b) Relative Col 1, Myl3, Myh6, and Mybpc3 gene expression in PBS, carrier, cell, and cell carrier groups ( $n = 4$ ). (c) Representative immunohistochemical images of vertically cross sectioned hearts stained with H&E and MT staining (scale bar = 2 mm). (d) Representative images of TUNEL- (green) and cTnT-positive (cardiomyocyte marker, red) signals in rat MI model after the treatments (scale bar = 200 μm). (e) Representative immunohistochemical images showing CD31-positive signals in rat MI model after the treatment. White arrow indicates the CD31-positive signal (scale bar = 100 μm). \* $p < 0.05$ , \*\* $p < 0.01$ , \*\*\* $p < 0.001$  compared to PBS group, ### $p < 0.01$  compared to each group.

group indicates reduced cardiac atrophy and suggests that the hydrogel scaffold with encapsulated cells effectively mitigated cardiac deterioration post-MI.

Moreover, enhanced expression of myocardial markers such as Col 1, Myl3, Myh6, and Mybpc3 in the cell carrier group suggests significant recovery of myocardial function. Histological analysis using H&E

and MT staining further reinforced these findings, showing improved cellular organization and reduced fibrosis in the cell carrier group. Furthermore, significant recovery of the ventricular cavity and wall thickness was observed in the cell carrier group (figure S4). In figure 7(d), the merged image of TUNEL- and cTnT-positive signals indicates that

the cell carrier group showed a significant increase in cTnT expression, reflecting enhanced cardiomyocyte survival and function (figure S5(a)). In contrast, TUNEL-positive apoptotic cells were prevalent in the PBS, carrier-only, and cell-only groups, whereas they were notably absent in the cell carrier group (figure S5(a)). This suggests that the cell-laden hydrogel not only supports myocardial regeneration but also effectively prevents cell death, which is critical for long-term cardiac repair. As shown in figure 7(e), immunohistochemical analysis of CD31, an endothelial marker, revealed weak expression in the carrier-only group, indicating limited angiogenesis. However, CD31 expression was significantly higher in the cell carrier group compared to all other groups (figure S5(b)), suggesting that the cell-laden hydrogel promotes angiogenesis, essential for supplying nutrients and oxygen to the regenerating myocardial tissue.

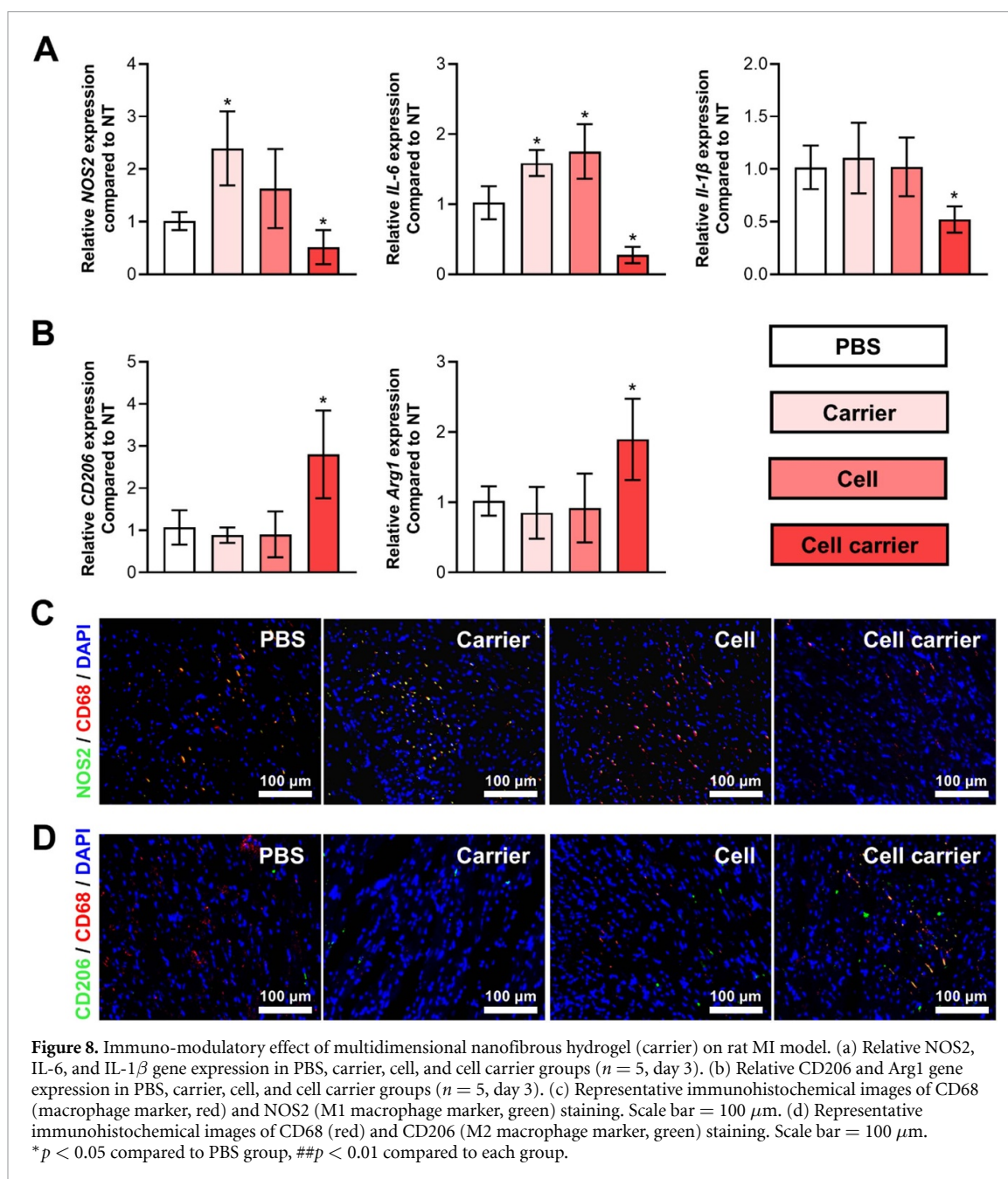
### 3.7. Evaluating immuno-modulatory effect of multidimensional nanofibrous hydrogel

The immune-modulatory effects of the cell-laden hydrogel carrier were analyzed by examining the expression levels of M1 and M2 macrophage markers. As shown in figure 8(a), the expression of M1 markers, including NOS2, IL-6, and IL-1 $\beta$ , was significantly lower in the cell carrier group compared to the PBS group, indicating suppression of the proinflammatory M1 macrophage response. The carrier-only and cell-only groups exhibited expression levels similar to or slightly higher than those in the PBS group, further highlighting the unique immune-modulatory effects of the cell-laden hydrogel. Conversely, figure 8(b) shows that the expression of M2 markers, CD206 and Arg1, was highest in the cell carrier group, indicating a shift toward the anti-inflammatory, tissue-repairing M2 macrophage phenotype. The carrier-only and cell-only groups did not display a significant difference in M2 marker expression compared to the PBS group. In addition to gene expression, tissue-level analysis of macrophage activation was conducted using immunohistochemical staining. As depicted in figures 8(c) and (d), M1 macrophage activation, marked by NOS2, was observed in all groups except the cell carrier group, where it was minimal (figure S5(c)). In contrast, M2 macrophage activation, marked by CD206, was significantly elevated in the cell carrier group, demonstrating a clear shift toward an anti-inflammatory response (figure S5(d)). These results confirm that the cell-laden hydrogel effectively modulates the immune environment at both the genetic and cellular levels, promoting a healing-oriented response that is critical for successful myocardial regeneration.

## 4. Discussion

Traditional strategies for myocardial repair, such as pharmacological treatments [36] and mechanical support devices [37], have primarily focused on symptom management rather than addressing the underlying loss of myocardial tissue. As a result, these approaches often fail to replicate the mechanical properties of the heart [38] or only incorporate some of the multicellular components [39]. This study demonstrates that the developed hydrogel effectively overcomes these limitations, offering a promising solution for myocardial regeneration.

The multidimensional design of the hydrogel, featuring the integration of PCL fibers within a fibrin matrix and encapsulation by an alginate layer, addresses a key limitation of previous scaffolds—the lack of mechanical strength combined with the ability to mimic the tissue microenvironment. This design also incorporates a triculture strategy using cardiac regenerative cells (ADSCs, HUVECs, and C2C12 cells). As shown in figures 2(a) and (b), the compartmentalization within the hydrogel provides distinct mechanical and biological functions. The compressive modulus of the hydrogels was measured to assess their mechanical robustness. As shown in figure 2(c), the fibrin hydrogel exhibited a compressive modulus of  $3.60 \pm 0.37$  kPa, indicating a relatively soft matrix suitable for cell proliferation but insufficient to withstand the dynamic mechanical forces of the heart [38]. The integration of PCL fibers significantly enhanced the compressive modulus to  $5.92 \pm 1.78$  kPa, providing greater structural integrity. Following the addition of an alginate coating, the compressive modulus further increased to  $33 \pm 8.31$  kPa, bringing the hydrogel into the range suitable for cardiac tissue applications. These findings are supported by dynamic rheology measurements (figure 2(d)), which demonstrated that the storage modulus of the PCL-embedded fibrin hydrogel with alginate coating remained consistently higher across all tested frequencies. The substantial increase in compressive modulus with the incorporation of PCL fibers and, notably, the alginate coating, highlights the hydrogel's ability to withstand the dynamic mechanical environment of the heart. Additionally, the hydrogel's high swelling capacity (figure 2(e)) enhances its ability to retain moisture, which is crucial for cellular survival and proliferation, addressing the dual challenges of mechanical robustness and biological functionality [40]. The integration of PCL fibers, along with the crucial addition of alginate, not only optimizes the mechanical properties of the hydrogel for cardiac tissue applications but also effectively addresses the dual challenges of maintaining mechanical robustness and biological functionality.



Our hydrogel system demonstrated a strong capacity to support cell survival and proliferation. The high viability and proliferation rates observed in ADSCs, HUVECs, and C2C12 cells (figure 3(a)) underscore the excellent biocompatibility of the hydrogel. Additionally, both direct and indirect assessments confirmed the absence of cytotoxicity, showing that the hydrogel does not negatively affect cell survival within the scaffold or the surrounding cells (figure 3(b)). One of the key aspects of myocardial regeneration is the promotion of angiogenesis, which ensures an adequate supply of oxygen and nutrients to the regenerating tissue. Previous approaches that involved co-culturing one or two cell types have often been limited in their ability to fully replicate the complexity of the disease environment,

ultimately constraining their success in promoting effective vascularization and tissue integration [41, 42]. The results of this study (figures 4 and 5) demonstrate that the 3D triculture system within the hydrogel significantly enhances the expression of wound healing and angiogenic factors, including HIF-1 $\alpha$  and VEGF [35], MMP1 [43], CD31 [44], and FGF2 [45] as shown in figures 4 and 5. These markers indicate that the hydrogel supports cell growth and actively promotes new blood vessel formation. In 2D normoxia, HIF-1 $\alpha$  and VEGF expression levels were baseline, whereas in 2D hypoxia, HIF-1 $\alpha$  expression increased by 3.79-fold and VEGF by 6.656-fold. In the 3D hydrogel, HIF-1 $\alpha$  expression increased 6.09-fold and VEGF expression 12.589-fold, suggesting that both the hypoxic environment and the 3D

structure contribute to VEGF upregulation, crucial for angiogenesis. The higher VEGF expression in 3D conditions implies that cell-cell and cell-matrix interactions in the hydrogel create a microenvironment that effectively mimics hypoxia, fostering additional VEGF expression.

The significant increase in angiogenesis observed in the tube formation assay (figure 5) underscores the hydrogel's potential to create a conducive environment for vascular network formation [44, 46]. Notably, the triculture of all three cell types demonstrated superior angiogenic potential compared to both the HUVECs monoculture and the HUVECs + ADSCs co-culture. When HUVECs were cultured alone within the hydrogel, the number of junctions and nodes was  $24.0 \pm 10.81$ , which was not significantly different from the control hydrogel without cells ( $24.33 \pm 6.35$ ). However, in the HUVECs + ADSCs co-culture, there was a significant increase in junctions ( $36.33 \pm 3.21$ ) and nodes, indicating an enhanced angiogenic response. The addition of C2C12 cells in the triculture system further amplified these effects, with the number of junctions increasing to  $41.0 \pm 6.0$ . This demonstrates that the triculture system, by providing a more complex multicellular environment, significantly improves the formation of a robust vascular network, which is essential for effective myocardial regeneration.

Managing the immune response to implanted biomaterials remains a critical challenge in cardiac tissue regeneration. Uncontrolled inflammation can lead to fibrosis and scaffold rejection, ultimately compromising the success of regenerative therapies [10]. As demonstrated in figures 6 and 8, our hydrogel system effectively modulates the immune response by promoting a transition from a pro-inflammatory M1 macrophage phenotype to an anti-inflammatory, tissue-repairing M2 phenotype, both *in vitro* and *in vivo* [47]. As shown in figure 6(a), the analysis of pro-inflammatory cytokines, including TNF- $\alpha$ , IL-6, and IL-1 $\beta$ , revealed that, unlike the control group, both the fibrin and fibrin-alginate coated hydrogels did not induce detectable levels of these inflammatory markers, indicating an absence of harmful inflammation. Specifically, TNF- $\alpha$  levels were  $399.56 \pm 49.48$  pg ml $^{-1}$  in the control group, but were undetectable in the fibrin and fibrin-alginate hydrogel groups. Similarly, IL-6 levels were  $108.67 \pm 32.84$  pg ml $^{-1}$  in the control group, with no detectable expression in the hydrogel-treated groups. Furthermore, the increased expression of M2 macrophage markers, such as CD206 and Arg1 (figure 8(b)), was confirmed at the *in vivo* level, highlighting the hydrogel's ability not only to prevent an inflammatory response but also to actively promote a healing-oriented immune environment. The body and heart weight data (figure 7(a)) provide compelling evidence that the cell-laden hydrogel effectively mitigates cardiac deterioration post-MI, leading to improved

overall health and cardiac function. The average body weight of MI-induced rats in the cell carrier group was  $280.67 \pm 9.04$  g, significantly higher than the  $254.83 \pm 11.89$  g in the NT group,  $258.08 \pm 10.05$  g in the carrier-only group, and  $251.33 \pm 16.88$  g in the cell-only group. This increase in body weight suggests that animals in the cell carrier group experienced less systemic deterioration and better overall health, likely due to improved cardiac function. Similarly, heart weight analysis showed that the average heart weight in the cell carrier group was  $1.52 \pm 0.14$  g, compared to  $1.22 \pm 0.06$  g in the NT group,  $1.23 \pm 0.05$  g in the carrier-only group, and  $1.21 \pm 0.08$  g in the cell-only group. The higher heart weight observed in the cell carrier group indicates reduced cardiac atrophy and further supports the conclusion that the hydrogel scaffold with encapsulated cells effectively mitigates cardiac deterioration post-MI. This is further reinforced by the enhanced expression of myocardial markers (figure 7(b)) Mybpc3 [48], Myh6 [49], and Myl3 [50], along with improved histological outcome (figure 7(c)). The prevention of apoptosis, as indicated by TUNEL staining (figure 7(d)), and the increase in cTnT expression, suggest that the hydrogel not only supports myocardial regeneration but also effectively prevents cell death, which is crucial for long-term functional recovery [51]. The robust angiogenesis, as evidenced by the significant increase in CD31 expression (figure 7(e)), further supports the notion that the hydrogel promotes the formation of a functional vascular network, which is essential for sustaining the regenerated myocardium.

In this study, we used C2C12 cells, a muscle cell line with advantages in cardiac regeneration, as part of our proof-of-concept approach. C2C12 cells offer several benefits, including ease of culture and adaptability in diverse environments, and have shown promising outcomes in cardiac tissue engineering. For example, C2C12 cells have been reported to integrate within biocompatible scaffolds that exhibit antioxidative properties and enhanced mechanical strength, providing a suitable environment for cardiac tissue applications [23]. Additionally, they have demonstrated potential for myotube differentiation and survival in the myocardium of syngeneic mice [25], alignment in microgrooved structures to mimic myocardial tissue [26], and cardiac-like sodium current properties in cardiac environments [52]. When co-cultured with endothelial cells like HUVECs, C2C12 cells further support angiogenesis, producing pro-angiogenic factors through extracellular vesicles and enhancing muscle regeneration markers such as MyoD, myogenin, MHC, and troponin T [53–55].

However, C2C12 cells lack the higher differentiation capacity and regenerative abilities of more cardiac-specific cells, such as iPSC-derived cardiomyocytes (iPSC-CMs), neonatal cardiomyocytes, or cardiac progenitor cells. Future research should focus

on utilizing primary cells with superior cardiomyogenic and regenerative properties to fully exploit this platform's potential as a cell therapy for myocardial regeneration.

## 5. Conclusions

This study presents a multidimensional nanofibrous hydrogel scaffold designed for myocardial regeneration, combining mechanical robustness and biological compatibility to address challenges in cardiac tissue repair. Composed of PCL fibers, fibrin gel, and an alginate coating, the scaffold demonstrates superior mechanical properties, stability, and high swelling capacity—crucial for sustaining cellular activities and promoting tissue formation. The scaffold supports the survival and proliferation of ADSCs, HUVECs, and C2C12 cells without inducing cytotoxicity, ensuring biocompatibility. Enhanced gene expression of MMP1, CD31, and FGF2 within the scaffold indicates a synergistic effect that promotes tissue regeneration and angiogenesis. Additionally, activation of the HIF-1 $\alpha$ /VEGF pathway supports angiogenesis and myocardial repair. *In vivo* studies using a rat MI model showed improved myocardial regeneration when the scaffold was applied with cells. Overall, the multidimensional nanofibrous hydrogel scaffold addresses the mechanical and biological demands of myocardial regeneration, offering significant potential as a therapeutic platform for cardiac tissue engineering and advancing regenerative therapies in cardiology.

## Data availability statement

The data cannot be made publicly available upon publication because no suitable repository exists for hosting data in this field of study. The data that support the findings of this study are available upon reasonable request from the authors.

## Acknowledgment

This research was supported by a Grant of Ministry of Trade, Industry, and Energy, Republic of Korea (No. 20018522), and a Grant of Korea Health Technology R&D Project through the Korea Health Industry Development Institute (KHIDI), funded by the Ministry of Health and Welfare, Republic of Korea (No. HI22C1394). This work has been financially supported by Korean Fund for Regenerative Medicine (KFRM) Grant funded by the Korea government (the Ministry of Science and ICT, the Ministry of Health & Welfare; Project Number: 21A0102L1-12) and the KIST Institutional Program (Project No. 2E32351, 2E32350 'Development of cellular bloc platform technology', Korea).

## Ethics Statement

The handling of all animals in this study was approved and certified by the Institutional Animal Care and Use Committee at Sungkyunkwan University (Approval No: SKKUIACUC2021-12-14-2). All procedures adhered to ethical guidelines to ensure animal welfare, with efforts made to reduce unnecessary stress, pain, and harm. The animals were provided with the five freedoms, allowing for natural behaviors, health, and well-being throughout their care. Species-specific management and treatment protocols were followed to prioritize the humane treatment of all animals involved in the study.

## Conflict of interest

The authors declare no conflicts of interest.

## ORCID iD

Kangwon Lee  <https://orcid.org/0000-0001-5745-313X>

## References

- [1] Nedkoff L, Briffa T, Zemedikun D, Herrington S and Wright F L 2023 Global trends in atherosclerotic cardiovascular disease *Clin. Ther.* **45** 1087–91
- [2] Tajabadi M, Orimi H G, Ramzgouyan M R, Nemati A, Deravi N, Beheshtizadeh N and Azami M 2022 Regenerative strategies for the consequences of myocardial infarction: chronological indication and upcoming visions *Biomed. Pharmacother.* **146** 112584
- [3] Henry T D *et al* 2021 Invasive management of acute myocardial infarction complicated by cardiogenic shock: a scientific statement from the american heart association *Circulation* **143** E815–29
- [4] Ravi P, Burch M B, Giannopoulos A A, Liu I S B L, Kondor S, Chepelev L L, Danesi T H, Rybicki F J and Panza A 2024 Desktop 3D printed anatomic models for minimally invasive direct coronary artery bypass *3D Print Med.* **10** 19
- [5] Zhang S J *et al* 2023 Minimally invasive direct coronary artery bypass versus percutaneous coronary intervention for isolated left anterior descending artery stenosis: an updated meta-analysis *Heart Surg. Forum* **26** E114–25
- [6] Liu N B *et al* 2021 Advances in 3D bioprinting technology for cardiac tissue engineering and regeneration *Bioact. Mater.* **6** 1388–401
- [7] Zhao X T, Li Q, Guo Z K and Li Z J 2021 Constructing a cell microenvironment with biomaterial scaffolds for stem cell therapy *Stem Cell Res. Ther.* **12** 583
- [8] Augustine R, Dan P, Hasan A, Khalaf I M, Prasad P, Ghosal K, Gentile C, McClements L and Maureira P 2021 Stem cell-based approaches in cardiac tissue engineering: controlling the microenvironment for autologous cells *Biomed. Pharmacother.* **138** 111425
- [9] Yan W J, Xia Y L, Zhao H S, Xu X M, Ma X L and Tao L 2024 Stem cell-based therapy in cardiac repair after myocardial infarction: promise, challenges, and future directions *J. Mol. Cell Cardiol.* **188** 1–14
- [10] Nguyen A H, Marsh P, Schmiess-Heine L, Burke P J, Lee A, Lee J and Cao H 2019 Cardiac tissue engineering: state-of-the-art methods and outlook *J. Biol. Eng.* **13** 57
- [11] Perez-Estena I *et al* 2022 A multimodal scaffold for tissue integration and SDF-1 delivery improves cardiac function in

- a rat model of subacute myocardial infarction *Eur. J. Heart Fail.* **24** 43–44
- [12] Della Rocca D G *et al* 2012 A degradable, bioactive, gelatinized alginate hydrogel to improve stem cell/growth factor delivery and facilitate healing after myocardial infarction *Med. Hypotheses* **79** 673–7
- [13] Moroni L and Elisseff J H 2008 Biomaterials engineered for integration *Mater. Today* **11** 44–51
- [14] Chen P H, Liao H C, Hsu S H, Chen R S, Wu M C, Yang Y F, Wu C C, Chen M H and Su W F 2015 A novel polyurethane/cellulose fibrous scaffold for cardiac tissue engineering *RSC Adv.* **5** 6932–9
- [15] Roshanbinfar K, Kolesnik-Gray M, Angeloni M, Schrufer S, Fiedler M, Schubert D W, Ferrazzi F, Krstic V and Engel F B 2023 Collagen hydrogel containing polyethylenimine-gold nanoparticles for drug release and enhanced beating properties of engineered cardiac tissues *Adv. Healthcare Mater.* **12** 2202408
- [16] Berry M F, Engler A J, Woo Y J, Pirolli T J, Bish L T, Jayasankar V, Morine K J, Gardner T J, Discher D E and Sweeney H L 2006 Mesenchymal stem cell injection after myocardial infarction improves myocardial compliance *Am. J. Physiol. Heart. Circ. Physiol.* **290** H2196–203
- [17] Negrini N C, Volponi A A, Higgins C A, Sharpe P T and Celiz A D 2021 Scaffold-based developmental tissue engineering strategies for ectodermal organ regeneration *Mater. Today Bio* **10** 100107
- [18] Laurens N, Koolwijk P and De Maat M P M 2006 Fibrin structure and wound healing *J. Thromb. Haemost.* **4** 932–9
- [19] Jarrell D K and Jacot J G 2023 An characterization of a PCL-fibrin scaffold for myocardial repair *Mater. Today Commun.* **37** 107596
- [20] Grijalvo S, Nieto-Díaz M, Maza R M, Eritja R and Díaz D D 2019 Alginate hydrogels as scaffolds and delivery systems to repair the damaged spinal cord *Biotechnol. J.* **14** 1900275
- [21] Abasalizadeh F, Moghaddam S V, Alizadeh E, Akbari E, Kashani E, Fazljou S M B, Torbati M and Akbarzadeh A 2020 Alginate-based hydrogels as drug delivery vehicles in cancer treatment and their applications in wound dressing and 3D bioprinting *J. Biol. Eng.* **14** 8
- [22] Bupphathong S, Lim J, Fang H W, Tao H Y, Yeh C E, Ku T A, Huang W, Kuo T Y and Lin C H 2024 Enhanced vascular-like network formation of encapsulated HUVECs and ADSCs coculture in growth factors conjugated GelMA hydrogels *ACS Biomater. Sci. Eng.* **10** 3306–15
- [23] Naveenkumar S, Venkateshan N, Kaviyarasu K, Christyraj J R S S and Muthukumar A 2023 Optimum performance of a novel biocompatible scaffold comprising alginate-pectin-selenium nanoparticles for cardiac tissue engineering using C2C12 cells *J. Mol. Struct.* **1294** 136457
- [24] Abud M B *et al* 2022 *In vivo* study to assess dosage of allogeneic pig retinal progenitor cells: long-term survival, engraftment, differentiation and safety *J. Cell Mol. Med.* **26** 3254–68
- [25] Koh G Y, Klug M G, Soonpaa M H and Field L J 1993 Differentiation and long-term survival of C2c12 myoblast grafts in heart *J. Clin. Invest.* **92** 1548–54
- [26] Wang Y, Cui H T, Wang Y C, Xu C Y, Esworthy T J, Hann S Y, Boehm M, Shen Y L, Mei D Q and Zhang L J R A C 2021 4D printed cardiac construct with aligned myofibers and adjustable curvature for myocardial regeneration *ACS Appl. Mater. Interfaces* **13** 12746–58
- [27] Wu P, Deng G, Sai X, Guo H M, Huang H L and Zhu P 2021 Maturation strategies and limitations of induced pluripotent stem cell-derived cardiomyocytes *Biosci. Rep.* **41** BSR20200833
- [28] Liu J, Chuah Y J, Fu J Y, Zhu W Z and Wang D A 2019 Co-culture of human umbilical vein endothelial cells and human bone marrow stromal cells into a micro-cavitary gelatin-methacrylate hydrogel system to enhance angiogenesis *Mater. Sci. Eng. C* **102** 906–16
- [29] Tan A W, Liao L L, Chua K H, Ahmad R, Akbar S A and Pinguan-Murphy B 2016 Enhanced *in vitro* angiogenic behaviour of human umbilical vein endothelial cells on thermally oxidized TiO nanofibrous surfaces *Sci. Rep.* **6** 21828
- [30] Hong C, Chung H, Lee G, Kim C, Kim D, Oh S J, Kim S H and Lee K 2023 Hydrogel/nanofiber composite wound dressing optimized for skin layer regeneration through the mechanotransduction-based microcellular environment *ACS Appl. Bio Mater.* **6** 1774–86
- [31] Hyun J, Yun D W, Um S H and Bhang S H 2024 Hypoxia potentiated pro-angiogenic and anti-fibrotic effect of nanovesicles derived from human mesenchymal stem cells *J. Ind. Eng. Chem.* **137** 514–23
- [32] Gil-Cabrerizo P, Scacchetti I, Garbayo E and Blanco-Prieto M J 2023 Cardiac tissue engineering for myocardial infarction treatment *Eur. J. Pharm. Sci.* **185** 106439
- [33] Kapalczynska M, Kolenda T, Przybyla W, Zajackowska M, Teresiak A, Filas V, Ibbs M, Blizniak R, Luczewski Ł and Lamperska K 2018 2D and 3D cell cultures—a comparison of different types of cancer cell cultures *Arch. Med. Sci.* **14** 910–9
- [34] Elomaa L, Lindner M, Leben R, Niesner R and Weinhart M 2023 vascularization of hydrogel-based tissue constructs via a combined approach of cell sheet engineering and dynamic perfusion cell culture *Biofabrication* **15** 015004
- [35] Du Y Q *et al* 2018 Hypoxia-inducible factor 1 alpha (HIF-1 $\alpha$ )/vascular endothelial growth factor (VEGF) pathway participates in angiogenesis of myocardial infarction in muscone-treated mice: preliminary study *Med. Sci. Monit.* **24** 8870–7
- [36] Sachdeva P *et al* 2023 Advancements in myocardial infarction management: exploring novel approaches and strategies *Cureus J. Med. Sci.* **15** 9
- [37] Chaggar P S, Williams S G, Yonan N, Fildes J, Venkateswaran R and Shaw S M 2016 Myocardial recovery with mechanical circulatory support *Eur. J. Heart Fail.* **18** 1220–7
- [38] Xu Q X, Xiao Z Y, Yang Q Z, Yu T T, Deng X J, Chen N H, Huang Y Y, Wang L H, Guo J and Wang J H 2024 Hydrogel-based cardiac repair and regeneration function in the treatment of myocardial infarction *Mater. Today Bio* **25** 100978
- [39] Litvinukova M *et al* 2020 Teichmann, cells of the adult human heart *Nature* **588** 466
- [40] Patra S K *et al* 2022 Prospects of hydrogels in agriculture for enhancing crop and water productivity under water deficit condition *Int. J. Polym. Sci.* **2022** 1–15
- [41] Liu X *et al* 2022 Bone tissue engineering scaffolds with HUVECs/hBMSCs cocultured on 3D-printed composite bioactive ceramic scaffolds promoted osteogenesis/angiogenesis *J. Orthop. Transl.* **37** 152–62
- [42] Kim D *et al* 2024 3D *in vitro* synovial hyperplasia model on polycaprolactone-micropatterned nanofibrous microwells for screening disease-modifying anti-rheumatic drugs *Mater. Today Bio* **26** 101061
- [43] Haas T L and Madri J A 1999 Extracellular matrix-driven matrix metalloproteinase production in endothelial cells: implications for angiogenesis *Trends Cardiovascular Med.* **9** 70–77
- [44] Lee S, Valmikinathan C M, Byun J, Kim S, Lee G, Mokarram N, Pai S B, Um E, Bellamkonda R V and Yoon Y S 2015 Enhanced therapeutic neovascularization by CD31-expressing cells and embryonic stem cell-derived endothelial cells engineered with chitosan hydrogel containing VEGF-releasing microtubes *Biomaterials* **63** 158–67
- [45] Jia T *et al* 2021 FGF-2 promotes angiogenesis through a SRSF1/SRSF3/SRPK1-dependent axis that controls VEGFR1 splicing in endothelial cells *BMC Biol.* **19** 1–26
- [46] Li Q, Cheng K, Wang A Y, Xu Q G, Fu Z F, He S Y and Xu P X 2019 microRNA-126 inhibits tube formation of HUVECs by

- interacting with and down-regulating PI3K/AKT signaling pathway *Biomed. Pharmacother.* **116** 109007
- [47] Chen S Q *et al* 2024 Modulation of anti-cardiac fibrosis immune responses by changing M2 macrophages into M1 macrophages *Mol. Med.* **30** 88
- [48] Rodríguez-García M I *et al* 2010 Screening mutations in myosin binding protein C3 gene in a cohort of patients with hypertrophic cardiomyopathy *BMC Med. Genet.* **11** 67
- [49] Zuo J Y, Chen H X, Liu Z G, Yang Q and He G W 2022 Identification and functional analysis of variants of gene promoter in isolated ventricular septal defects *BMC Med. Genomics* **15** 213
- [50] Yajima Y, Hiratsuka T, Kakimoto Y, Ogawa S, Shima K, Yamazaki Y, Yoshikawa K, Tamaki K and Tsuruyama T 2018 Region of Interest analysis using mass spectrometry imaging of mitochondrial and sarcomeric proteins in acute cardiac infarction tissue *Sci. Rep.* **8** 7493
- [51] Moridi M, Magnusson C and Zilg B 2022 Cardiac troponin T as a postmortem biomarker for acute myocardial infarction *Forensic. Sci. Int.* **341** 111506
- [52] Zebedin E, Mille M, Speiser M, Zarrabi T, Sandtner W, Latzenhofer B, Todt H and Hilber K 2007 Skeletal muscle cells adopt cardiac-like sodium current properties in a cardiac cell environment *Am. J. Physiol. Heart. Circ. Physiol.* **292** H439–50
- [53] Gholobova D, Decroix L, Van Muylder V, Desender L, Gerard M, Carpentier G, Vandeburgh H and Thorrez L 2015 Endothelial network formation within human tissue-engineered skeletal muscle *Tissue Eng. A* **21** 2548–58
- [54] Kargl C K *et al* 2023 Angiogenic potential of skeletal muscle derived extracellular vesicles differs between oxidative and glycolytic muscle tissue in mice *Sci. Rep.* **13** 18943
- [55] Yeo M and Kim G 2020 Micro/nano-hierarchical scaffold fabricated using a cell electrospinning/3D printing process for co-culturing myoblasts and HUVECs to induce myoblast alignment and differentiation *Acta Biomater.* **107** 102–14